Available online at www.sciencedirect.com
ScienceDirect
Journal of Power Sources 179 (2008) 474–480
JOURNAL OF POWER SOURCES
www.elsevier.com/locate/jpowsour

$(La_{0.74}Bi_{0.10}Sr_{0.16})MnO_{3-\delta}$–$(Bi_2O_3)_{0.7}(Er_2O_3)_{0.3}$ composite cathodes for intermediate temperature solid oxide fuel cells

Junliang Li *, Shaorong Wang *, Zhengrong Wang, Renzhu Liu, Tinglian Wen, Zhaoyin Wen

Shanghai Institute of Ceramics, Chinese Academy of Sciences, 1295 Dingxi Road, Shanghai 200050, PR China

Received 25 December 2007; accepted 7 January 2008
Available online 16 January 2008

Abstract

$(La_{0.74}Bi_{0.10}Sr_{0.16})MnO_{3-\delta}$ (LBSM)–$(Bi_2O_3)_{0.7}(Er_2O_3)_{0.3}$(ESB) composite cathodes were fabricated for intermediate-temperature solid oxide fuel cells with Sc-stabilized zirconia as the electrolyte. The performance of these cathodes was investigated at temperatures below 750 °C by AC impedance spectroscopy and the results indicated that LBSM–ESB had a better performance than traditional composite electrodes such as LSM–GDC and LSM–YSZ. At 750 °C, the lowest interfacial polarization resistance was only 0.11 Ω cm^2 for the LBSM–ESB cathode, 0.49 Ω cm^2 for the LSM–GDC cathode, and 1.31 Ω cm^2 for the LSM–YSZ cathode. The performance of the cathode was improved gradually by increasing the ESB content, and the performance was optimal when the amounts of LBSM and ESB were equal in composite cathodes. This study shows that the sintering temperature of the cathode affected performance, and the optimum sintering temperature for LBSM–ESB was 900 °C.

Keywords: Intermediate-temperature solid oxide fuel cells; Sintering temperature; Impedance spectroscopy; Composite cathode

1. Introduction

$La_{1-x}Sr_xMnO_3$ (LSM) perovskite is regarded as one of the most promising materials for solid oxide fuel cell (SOFC) cathodes because of its high levels of thermal and chemical stability. However, due to its low oxide ionic conductivity and high activation energy for oxygen disassociation, LSM is not suitable for SOFCs operating at temperatures below 800 °C. One commonly used means for improving electrode performance in SOFCs is to add an ionically conducting second phase to the electronically conducting electrode materials [1,2]. For example, yttria-stabilized zirconia (YSZ) is often mixed with strontium-doped lanthanum manganite (LSM), resulting in interfacial resistance (R) values significantly lower than that of single-phase LSM cathodes [2–6]. Murray et al. and Hui Zhao et al. reported the interfacial polarization resistance (area-specific resistance) at 700 °C decreased from 7.82 Ω cm^2 for an LSM cathode to 2.49 Ω cm^2 for an LSM–YSZ cathode, and further down to 1.78 Ω cm^2 and 1.06 Ω cm^2 for the LSM–CBO ($Ce_{0.7}Bi_{0.3}O_2$) and the LSM–GDC cathode, respectively [7,8]. It is believed that the cathode properties can be improved by increasing the triple phase boundary (TPB) formed on the electrolyte/electrode interface. For this purpose, the ionic conducting material should have a high level of conductivity at low temperature. It has been shown that the LSM–CGO composite electrode always has a better performance than that of LSM–YSZ, due to the much higher oxide ion conductivity of CGO at low temperature. Although the LSM–CGO composite cathode has much improved catalytic properties, searching for alternative materials is still attractive. Bismuth-based oxides have been investigated recently as possible cathode materials in IT-SOFC [9]. Doped bismuth oxide systems have high levels of oxide ion conductivity [10]. For instance, Er_2O_3-stabilized Bi_2O_3 (ESB) has the highest level of oxygen ion conductivity (0.37 S cm^{-1} at 973 K) [11,12] and is expected to improve the cathode performance by playing the role of CGO or YSZ.

This study was designed to examine the composite cathodes of the $(La_{0.74}Bi_{0.10}Sr_{0.16})MnO_{3-\delta}$–$(Bi_2O_3)_{0.7}(Er_2O_3)_{0.3}$ (LBSM–ESB) system. Bi_2O_3 is an effective sintering aid [13] and these composite cathodes have good sintering properties. We

* Corresponding authors. Tel.: +86 21 52411520; fax: +86 21 52413903.
E-mail address: srwang@mail.sic.ac.cn (S. Wang).

0378-7753/$ – see front matter © 2008 Elsevier B.V. All rights reserved.
doi:10.1016/j.jpowsour.2008.01.017

examined the effect of sintering temperature on the polarization resistance of the composite cathode.

2. Experimental

The $(La_{0.74}Bi_{0.10}Sr_{0.16})MnO_{3-\delta}$ (LBSM) powder was synthesized by autoignition of citrate–nitrate gel as described [13–15]. $La(NO_3)_3{\cdot}6H_2O$ (>99.0%), $Sr(NO_3)_2$ (>99.5%), and $Mn(NO_3)_2{\cdot}4H_2O$ (>99.0%) in stoichiometric proportions were mixed together in a water-bath at 80 °C. When they were dissolved completely, a certain amount of citric acid was introduced to form the LSM precursor solution. $Bi(NO_3)_3{\cdot}5H_2O$ (>99.0%) in stoichiometric proportion was dissolved in diluted nitric acid solution. The solution of $Bi(NO_3)_3$ was added to the LSM precursor solution, mixed and dried. The dry material was sintered in air at 850 °C for 6 h. The $(Bi_2O_3)_{0.7}(Er_2O_3)_{0.3}$ (ESB) powder was synthesized by the conventional solid reaction. Stoichiometric amounts of Bi_2O_3 (>99.99%) and Er_2O_3 (>99.9%) were mixed with ethanol and zirconia balls in a planetary ball mill for 3 h, then dried and heated at 750 °C in air for 10 h. The product was ball-milled again for 2 h to disrupt any aggregate.

LBSM–ESB mixtures were prepared by mixing LBSM powder with an appropriate amount of ESB (20 wt.%, 30 wt.%, 40 wt.%, 50 wt.% and 60 wt.%, corresponds to 15.74 vol.%, 24.25 vol.%, 33.24 vol.%, 42.76 vol.% and 52.84 vol.%, named LBSM–ESB1, LBSM–ESB2, LBSM–ESB3, LBSM–ESB4 and LBSM–ESB5, respectively). Some of the LBSM–ESB4 powder mixture was sintered in air at 1000 °C for 10 h in order to determine the chemical compatibility of LBSM and ESB. The LBSM and LBSM–ESB4 powders were pressed uniaxially into a cylinder 5 mm in diameter and ~20 mm in length to measure electrical conductivity. LBSM was sintered at 1200 °C for 10 h and LBSM–ESB4 was sintered at 1000 °C for 12 h in air. The density was greater than 93% of the theoretical value for the two materials. Electrical conductivity was measured by the standard four-probe DC method. Measurements were made in air from 500 °C to 750 °C with an interval of 50 °C.

Electrolyte-supported symmetric cells for impedance study were fabricated by screen printing the slurries of LBSM–ESB onto both sides of ScSZ electrolyte slices. The symmetric cells were sintered at 900 °C for 2 h in air. The area of each electrode was 1 cm^2. Silver mesh, attached to the cathode surface with silver paste, was used as the current collector. A four-probe configuration was used for electrochemical impedance spectroscopy (EIS) measurements.

Various phases of the powder were identified with a Rigaku X-ray diffraction (XRD) diffractometer at room temperature, using monochromatic Cu Kα radiation. The electrochemical performance of the cathodes was characterized at 500 °C, 550 °C, 600 °C, 650 °C, 700 °C, and 750 °C in air by EIS at open circuit, using AC impedance spectroscopy (ZAHNER IM6e) with a 20 mV AC signal, over a frequency range of 0.05 Hz to 1 MHz. The microstructure of the LBSM–ESB/ScSZ section was studied by scanning electron microscopy (SEM).

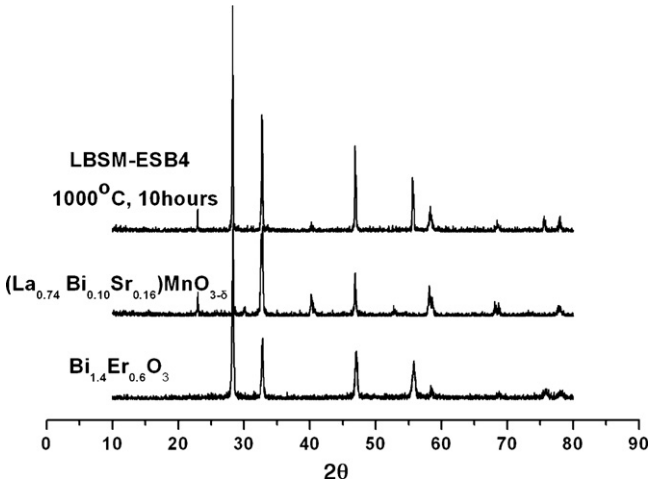

Fig. 1. XRD pattern of LBSM–ESB composite materials sintered at 1000 °C for 10 h.

3. Results and discussion

3.1. X-ray diffraction analysis

It has been reported that LSM reacts with YSZ to form the insulator phase $La_2Zr_2O_7$, which in turn has a negative effect on the electrochemical properties of the LSM–YSZ composite cathode. So, it is necessary to know the compatibility of LBSM with ESB. Fig. 1 shows the X-ray diffraction (XRD) pattern of the LBSM–ESB4 composite material. It was observed that the initial mixed powders gave the typical XRD patterns coming from LBSM and ESB in solid solution. No other phase was observed after the mixture was heated at 1000 °C for 10 h and we concluded, therefore, that the LBSM–ESB composite material is stable under the experimental conditions.

3.2. Electrical conductivity

The electrical conductivity of pure LBSM was higher than that of LBSM–ESB4 at the same temperature (Table 1). The disparity increased with decreased temperature. For example, at 750 °C, the electrical conductivity of LBSM and LBSM–ESB4

Table 1
Electrical conductivity of LBSM and LBSM–ESB4 at different temperatures

	Temperature					
	750 °C	700 °C	650 °C	600 °C	550 °C	500 °C
Conductivity of LBSM (S cm^{-1})	158	154	145	139	135	130
Conductivity of LBSM–ESB4 (S cm^{-1})	145	138	127	117	104	95

was 158 S cm^{-1} and 145 S cm^{-1}, respectively, and at 650 °C, the values were decreased to 145 S cm^{-1} and 127 S cm^{-1}, respectively. The electrical conductivity should be acceptable for the cathode at ~700 °C.

3.3. Effect of ESB content

Fig. 2a–f shows typical cross-section SEM images of cathodes sintered at 900 °C, with the electrolyte at the left. As shown in Fig. 2a and b, the screen-printed LBSM layer is highly porous, and the LBSM particles are uniform in size, which would be of great benefit for higher levels of cathode stability. In comparison, the SEM images of LBSM–ESB2 and LBSM–ESB4 cathodes are shown in Fig. 2c–f. After its introduction, ESB was seen to be surrounded with submicrometer particles, which are revealed to be LBSM by comparing Fig. 2d and f with Fig. 2b. As shown in Fig. 2c and d, ESB is completely covered with LBSM particles when 24.25 vol.% (30 wt.%) ESB is introduced into the compos-

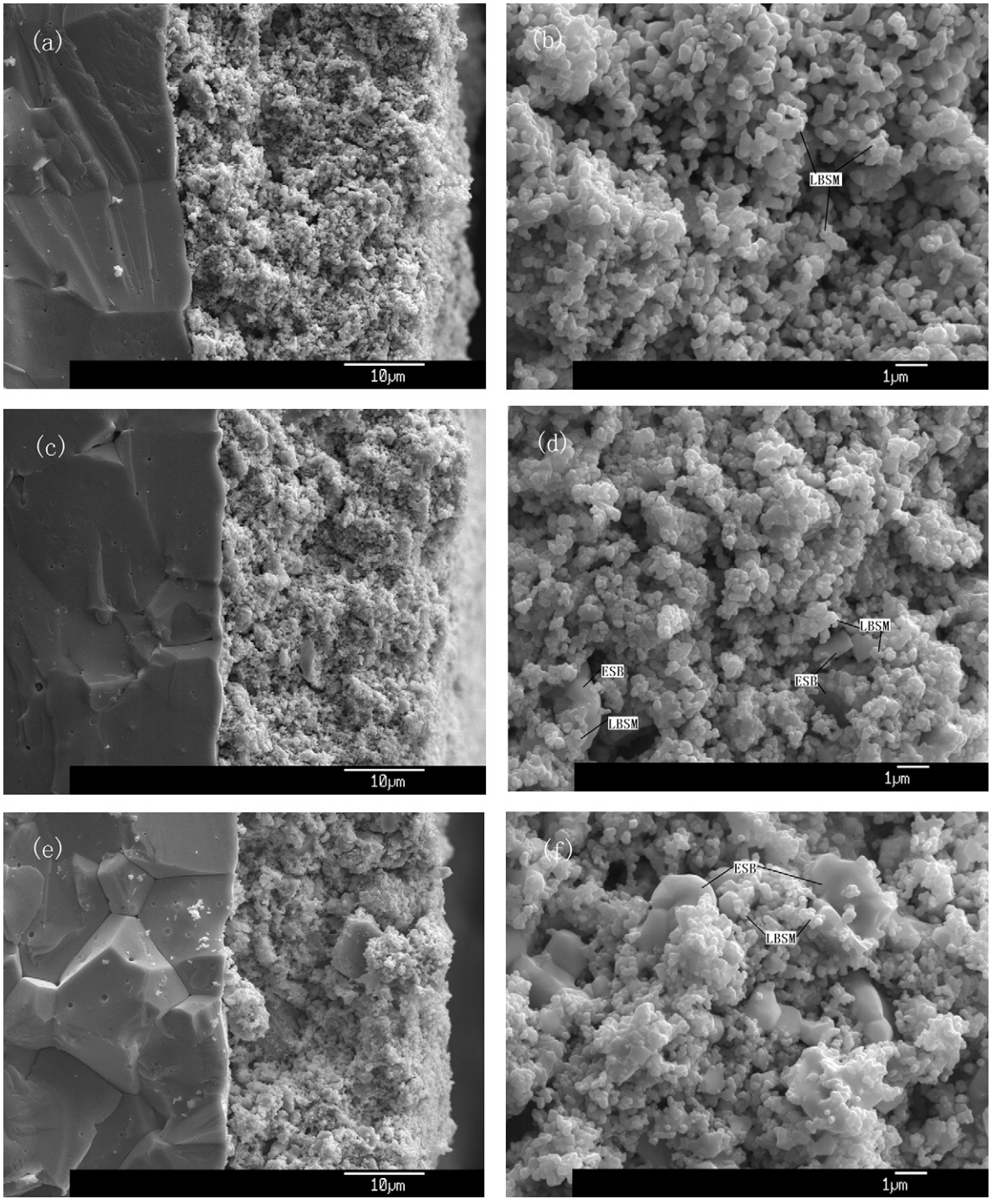

Fig. 2. Typical fracture cross-section SEM images of pure LBSM (a) and (b), LBSM–ESB2 (c) and (d), and LBSM–ESB4 (e) and (f) composite cathodes sintered at 900 °C.

ite cathode. So, ESB is in an isolated cluster and cannot provide sufficient ion transferring access. When 42.76 vol.% (50 wt.%) ESB is introduced, all the ESB particles are surrounded with LBSM, and the LBSM particles are still completely connected with each other (Fig. 2e–f). The mutual surrounding of ionic conduction phase and electronic conduction phase is assumed to effectively extend the triple phase boundary (TPB) and, consequently, enhance the electrochemical activity of the LBSM–ESB cathodes.

Fig. 3a–c shows impedance diagrams measured in air at 750 °C, 700 °C, and 650 °C for LBSM, LBSM–ESB2, and LBSM–ESB4, respectively. The equivalent circuit is presented in Fig. 3d, modeled as the arc for LBSM–ESB2. Pure LBSM and LBSM–ESB4 are also modeled well by this circuit. The promotion of cathode activity can be seen in Fig. 3a–c, where the impedance spectra are compared. The difference between real-axis intercepts of the impedance plot is considered to be the electrode polarization resistance R, which is decreased as the ESB content increased. Significant enhancement of the electrochemical activity for LBSM–ESB cathodes is clearly a result of the introduction of ESB. Therefore, one factor that contributed to the improved performance of the composite cathode was an increase of the ionic transport rate.

It is noted that the impedance spectra include a depressed semicircle in the low-frequency section and a minor high-frequency arc. The low-frequency semicircle comprises the chief contributing element in Fig. 3a–c. It has been suggested that the low-frequency semicircle can be attributed to oxygen adsorption and desorption on the electrode surface and the diffusion of oxygen ions [16–18]. On the other hand, the high-frequency arc can be attributed to polarization during charge transfer. In the equivalent circuit (Fig. 3d), the inductance L is attributed to high-frequency artifacts arising from the measurement apparatus. The first resistance (R_0) corresponds to the resistance of the electrolyte and the lead wires. The second resistance (R_1) is interpreted as the charge transfer resistance, which is contributed by electrochemical reaction at the cathode–electrolyte interface. Values of R_1 at 700 °C for LBSM, LBSM–ESB2, and LBSM–ESB4 cathodes were 1.28 Ω cm^2, 0.095 Ω cm^2, and 0.09 Ω cm^2, respectively. The Warburg impedance (W) is related to the resistance of oxygen adsorption/decomposition and the diffusion of oxygen ions in the cathode. Values of W at 700 °C for LBSM, LBSM–ESB2 and LBSM–ESB4 cathodes were 4.01 Ω cm^2, 0.22 Ω cm^2 and 0.12 Ω cm^2, respectively. The percentage for W in the total polarization resistance of the three composite cathodes decreased with increased ESB volume con-

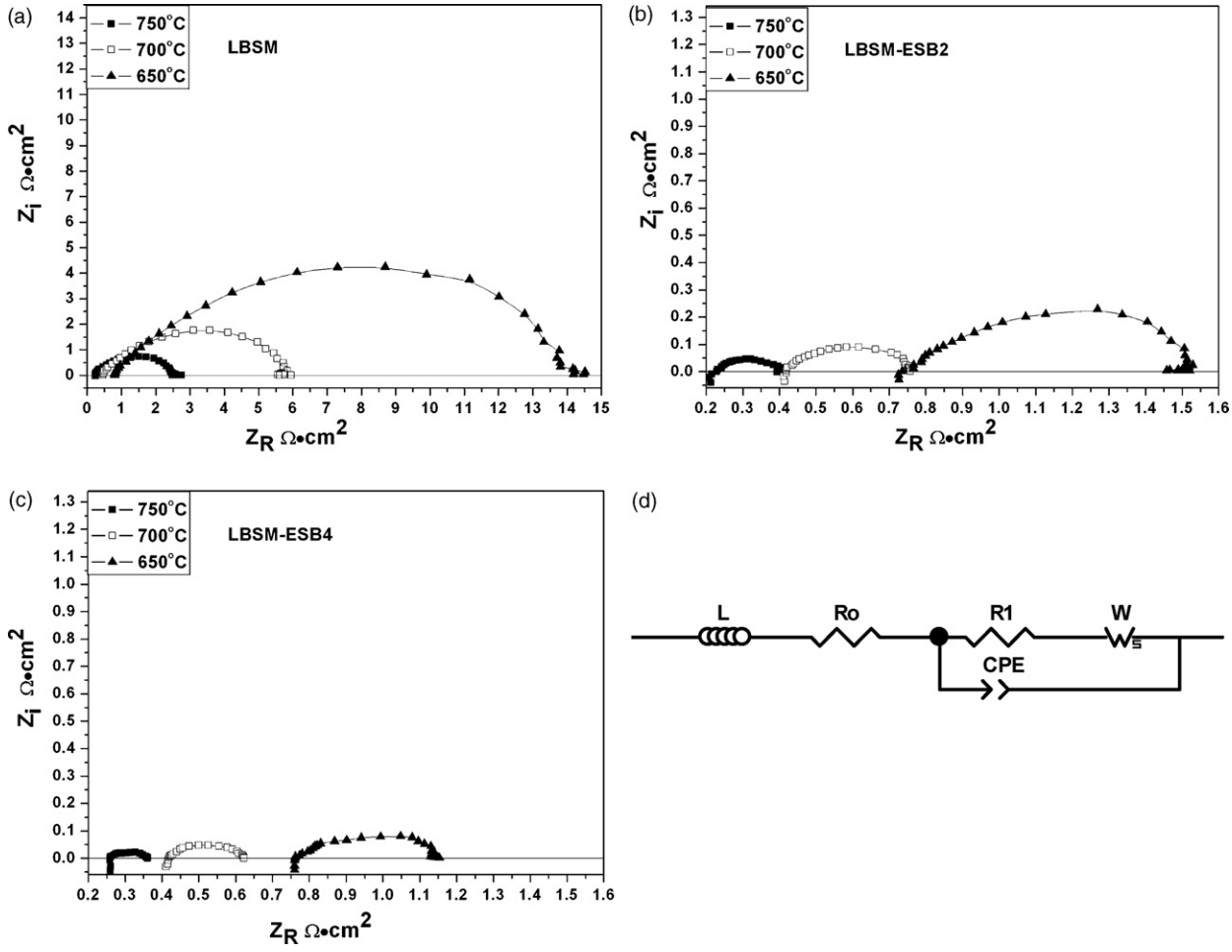

Fig. 3. AC impedance spectra measured at 650 °C, 700 °C, and 750 °C for pure LBSM (a), LBSM–ESB2 (b) and LBSM–ESB4 (c) cathodes. (d) Equivalent circuit model.

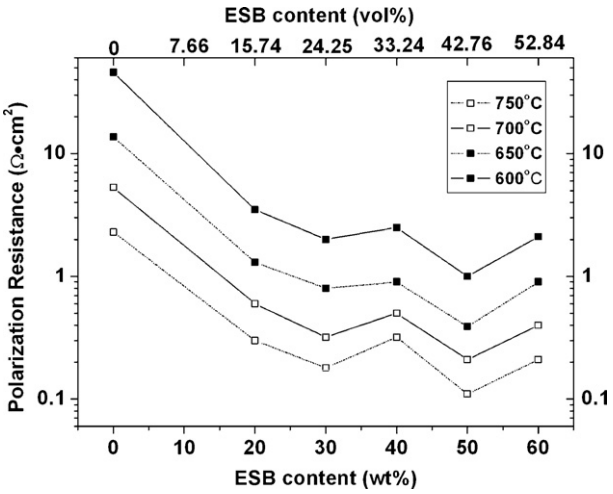

Fig. 4. Polarization resistance of LBSM–ESB composite cathodes with various ESB contents.

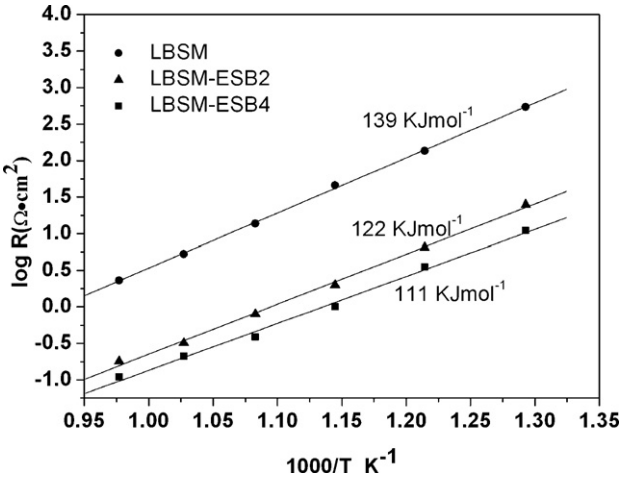

Fig. 5. Arrhenius plot of the polarization resistance of LBSM, LBSM–ESB2 and LBSM–ESB4 cathodes sintered at 900 °C.

tent. CPE is a constant phase element. The value of capacitance is $\sim 10^{-5}$ F and varies weakly with temperature in the three composite cathodes.

Fig. 4 summarizes the total polarization resistance R (the difference between the real-axis intercepts of the impedance arcs) for each of the LBSM–ESB cathodes measured in air. In general, the interfacial polarization resistance decreased as the ESB content increased to 42.76 vol.% (50 wt.%), except for a small deviation with 33.24 vol.% (40 wt.%) ESB content. R increased, however, for a further increase of ESB content to 52.84 vol.% (60 wt.%). This may be due to a decrease in the continuity of the LBSM phase in the composite, and hence a decrease in electronic transfer access. There is little polarization resistance when the ionic and electronic transportation phases are formed at an appropriate rate. The pure LBSM cathode yielded $R = 2.3\,\Omega\,cm^2$ and $5.3\,\Omega\,cm^2$ at 750 °C and 700 °C, and the LBSM–ESB2 cathode yielded $R = 0.18\,\Omega\,cm^2$ and $0.32\,\Omega\,cm^2$ at 750 °C and 700 °C. The optimal composition, LBSM–ESB4, yielded $R = 0.11\,\Omega\,cm^2$ and $0.21\,\Omega\,cm^2$ at 750 °C and 700 °C, respectively, and LSM–GDC50 yielded $R = 0.49\,\Omega\,cm^2$ and $1.06\,\Omega\,cm^2$ at 750 °C and 700 °C, respectively. So, the polarization of LBSM-ESB4 is a factor of four to five times lower than that of LSM–GDC50 cathodes [7]. Moreover, the LBSM–ESB50 value was about 20 times lower than the polarization resistance for pure LBSM. The greater effect of ESB than that of GDC on cathode performance can be explained, at least in part, by the higher ionic conductivity of ESB [19,20]. The high performance that resulted from the introduction of ESB was due to the uniform distribution of the electronic conducting particles in the ionic conducting structure and at the electrode/electrolyte interface (e.g. Fig. 2e and f), which simultaneously provided the effective ionic and electronic conducting paths and, at the same time, promoted the synergistic process involving the injection of the mobile charged oxygen species into the ionic carriers.

The activation energy can be calculated from the relationship of polarization resistance *versus* temperature shown in Fig. 5. The activation energy was 139 kJ mol^{-1}, 122 kJ mol^{-1} and 111 kJ mol^{-1} for the LBSM, LBSM–ESB2, and LBSM–ESB4 electrodes, respectively. The activation energy for LBSM–ESB2 and LBSM–ESB4 was lower than those of the other cathode materials. For example, the activation energy for LSM–YSZ was estimated to be 144 kJ mol^{-1} [21], which is approximately the value for the activation energy of pure LBSM. Thus, LBSM–ESB2 and LBSM–ESB4 would be expected to show lower polarization resistance than LSM–YSZ, especially at lower temperatures. The excellent performance obtained for the LBSM–ESB electrodes can be attributed to its high level of oxygen ion conductivity. In addition, the activation energies for oxygen ion diffusion and the oxygen surface exchange reaction are known to be 42(±2) kJ mol^{-1} and 113(±11) kJ mol^{-1}, respectively [22]. The activation energy for LBSM–ESB2 and LBSM–ESB4 is similar to that of the oxygen surface exchange reaction, and thus we suggest that the rate-determining step of the electrode reaction may be an oxygen surface exchange reaction, which is compatible with the equivalent circuit in Fig. 3d.

3.4. Effect of sintering on polarization resistance

As each reaction was affected by the microstructure of the electrode, the sintering temperature had a significant influence on the polarization resistance. Fig. 6 shows the relationship of the total polarization resistance of LBSM–ESB4 with sintering temperature. It was observed that sintering at 900 °C results in the minimum polarization resistance. Fig. 7 shows the impedance spectra of the composite cathodes that were sintered at different temperatures for 2 h and then measured at 700 °C in air. The values of polarization resistances were $0.7\,\Omega\,cm^2$, $0.40\,\Omega\,cm^2$, $0.21\,\Omega\,cm^2$ and $0.34\,\Omega\,cm^2$ for sintering temperatures 800 °C, 850 °C, 900 °C, and 950 °C, respectively. Fig. 8a–c shows the SEM images of fractured cross-sections of samples sintered at 800 °C, 900 °C, and 950 °C, and it can be observed that the ESB particles in composite cathodes grow with increasing sintering temperature. The ESB particle size in the composite cathode sintered at 800 °C is about 1 μm in diameter, and this increased to 3–4 μm at sintering temperatures up to 950 °C. Meanwhile,

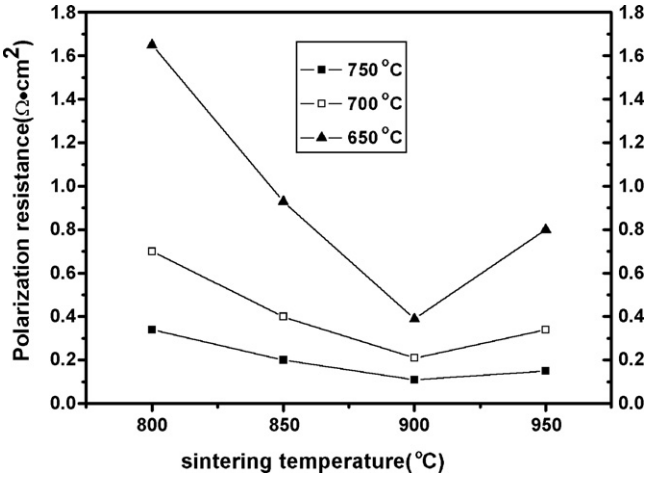

Fig. 6. Polarization resistance of LBSM–ESB4 with sintering temperature.

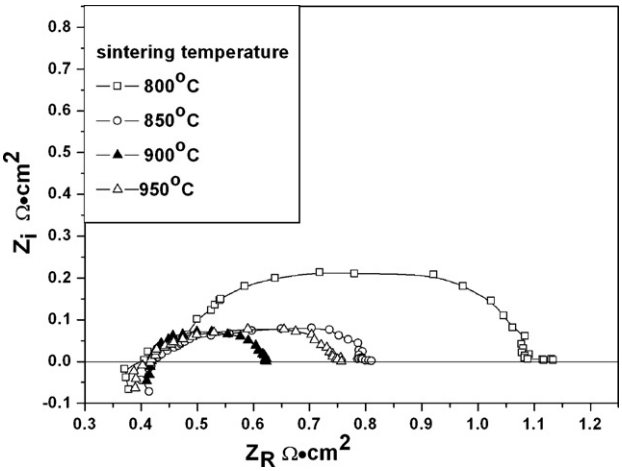

Fig. 7. AC impedance spectra of LBSM–ESB4 composite cathode sintered at different temperatures for 2 h and then measured at 700 °C in air.

LBSM particles were partially aggregated with increased sintering temperature.

The impedance spectra in Fig. 7 show that the total polarization resistance was relatively high when the electrode was sintered at 800 °C. The high polarization resistance may be attributed tentatively to the low sintering temperature and therefore the poor contact between the LBSM–ESB4 composite cathode and electrolyte (Fig. 8a). Similar phenomena have been observed for the LSM–YSZ composite cathode [23]. The total polarization resistance was reduced when the sintering temperature was 900 °C. Considering the low melting point of ESB powders, it is possible that a better contact was formed between LBSM and ESB particles, as well as the electrode–electrolyte

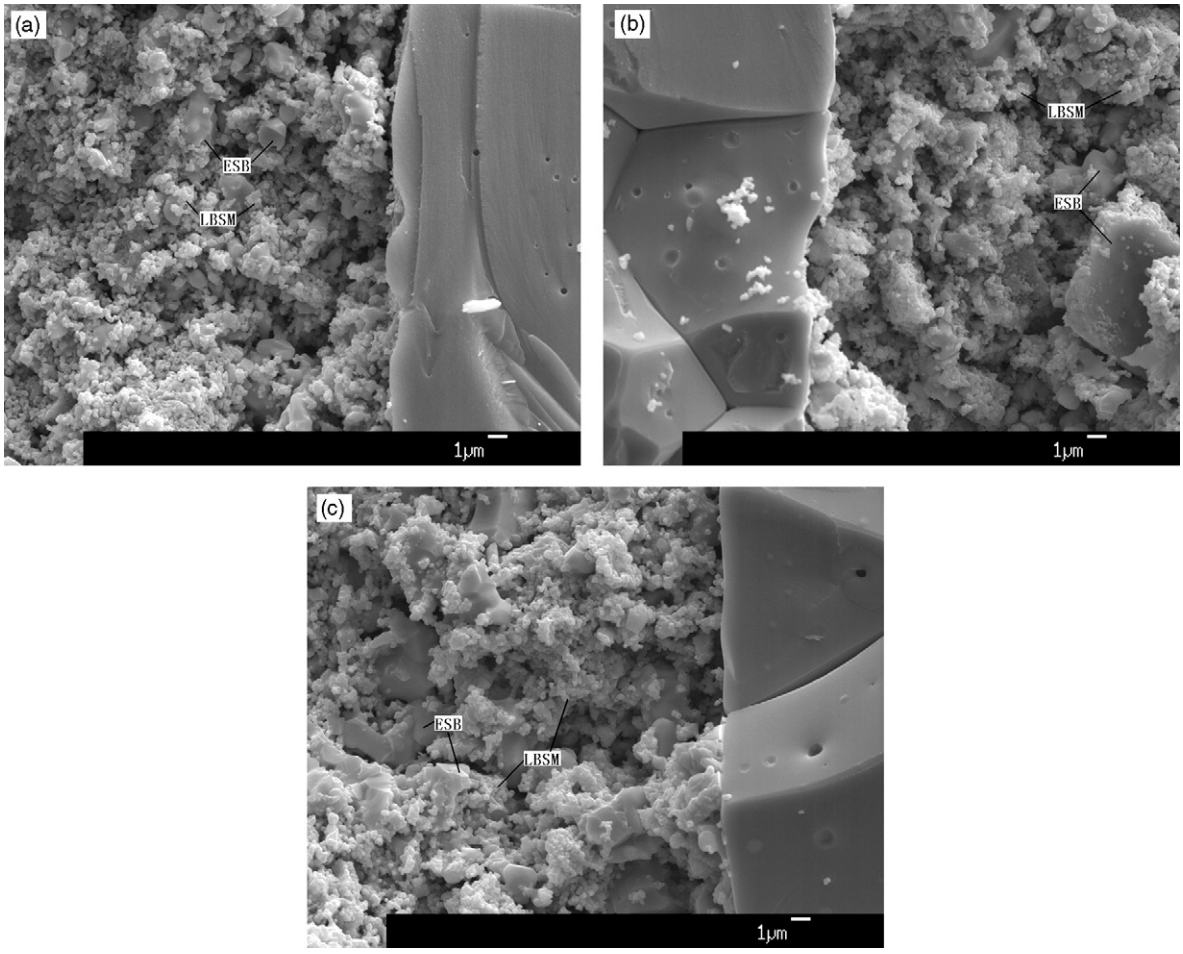

Fig. 8. Typical fracture cross-section SEM images of LBSM–ESB4 cathode sintered at 800 °C (a), 900 °C (b), and 950 °C (c).

interface at this temperature, which in turn reduced the interface resistance. When the sintering temperature was raised to 950 °C, however, the polarization resistance increased again. According to Fig. 8c, it may be due to over-sintering of the LBSM–ESB4 composite cathode. In this case, the ESB particles grew further and the LBSM particles were partially aggregated, which decreased the cathode porosity and reduced the gas diffusion rate. The TPB in the LBSM–ESB4 composite cathode and on the cathode–electrolyte interface were also decreased. Consequently, the performance was weakened and the cathode had a higher polarization resistance.

It may be possible to improve the performance of the LBSM–ESB cathodes. For example, performance could be improved by optimizing the cathode thickness. The cathode described here is about 25 μm thick. Earlier LSM–YSZ cathodes were suggested to have an optimum thickness of about 40 μm [4]. Since the conductivity of ESB exceeds that of YSZ, the optimum thickness may be greater [7,8]. We could change the approach of introducing ESB, such as an ion-impregnating process instead of mixing directly. Xu et al. reported the ion-impregnating process to be very beneficial to cathode performance [24]. In this case, the final sintering temperature could be reduced, and the ESB growth and the aggregation of LBSM particles would be reduced.

4. Conclusion

The characteristics of LBSM–ESB composite cathodes were investigated by AC impedance spectroscopy. The polarization resistance was decreased by incorporating an ionic conducting phase (ESB) in the electronic conducting phase (LBSM). Although the introduction of ESB decreased the electrical conductivity of the cathode at 750 °C (158 S cm^{-1} for LBSM and 145 S cm^{-1} for LBSM–ESB4), it resulted in a significant reduction of the polarization resistance from 2.3 Ω cm^2 for pure LBSM cathode to 0.11 Ω cm^2 for an LSM–ESB4 composite cathode at 750 °C. The microstructure of the LBSM–ESB4 composite cathode, varied in this study by changes of sintering temperature, was identified as having a significant effect on polarization, and the minimum polarization resistance was observed at a sintering temperature of 900 °C.

Acknowledgement

This work is supported financially by Chinese High Technology Development Project (2003AA517010).

References

[1] T. Kenjo, S. Osawa, K. Fujikawa, J. Electrochem. Soc. 138 (1991) 349–355.
[2] C.W. Tanner, K.Z. Fung, A.V. Virkar, J. Electrochem. Soc. 144 (1997) 21–30.
[3] T. Tsai, S.A. Barnett, Solid State Ionics 93 (1997) 207–217.
[4] E.P. Murray, T. Tsai, S.A. Barnett, Solid State Ionics 110 (1998) 235–243.
[5] M.J.L. Ostergard, C. Clausen, C. Bagger, M. Mogensen, Electrochem. Acta 40 (1995) 1971–1981.
[6] M. Juhl, S. Primdahl, C. Manon, M. Mogensen, J. Power Sources 61 (1996) 173–181.
[7] E.P. Murray, S.A. Barnett, Solid State Ionics 143 (2001) 265–273.
[8] H. Zhao, L. Huo, S. Gao, J. Power Sources 125 (2004) 149–154.
[9] H. Zhao, M. Pijolat, J. Mater. Chem. 12 (2002) 3787–3791.
[10] N.M. Sammes, G.A. Tompsett, H. NaÈ fe, F. Aldinger, J. Eur. Ceram. Soc. 19 (1999) 1801–1826.
[11] J.R. Jurado, C. Moure, P. Duran, N. Valverde, Solid State Ionics 28 (1988) 518–523.
[12] M.J. Verkerk, A.J. Burggraaf, J. Electrochem. Soc. 128 (1981) 75–82.
[13] A. Chakraborty, H.S. Maiti, Ceram. Int. 25 (1999) 115–123.
[14] A. Chakraborty, P.S. Devi, H.S. Maiti, Mater. Lett. 20 (1994) 63–69.
[15] A. Chakraborty, P.S. Devi, H.S. Maiti, J. Mater. Res. 10 (1995) 918–925.
[16] F.H. Heuveln, H.J.M. Bouwmeester, J. Electrochem. Soc. 144 (1997) 134–137.
[17] Y.J. Leng, S.H. Chan, K.A. Khor, S.P. Jiang, Int. J. Hydrogen Energy 29 (2004) 1025–1033.
[18] S. Li, Z. lü, N. Ai, K. Chen, W. Su, J. Power Sources 165 (2007) 97–101.
[19] B.C.H. Steele, Solid State Ionics 75 (1995) 157–165.
[20] M.J. Verkerk, K. Keizer, A.J. Burggraaf, J. Appl. Electrochem. 10 (1980) 81–90.
[21] N.T. Hart, N.P. Brandon, M.J. Day, N. Lapeñ-Rey, J. Power Sources 106 (2002) 42–50.
[22] S. Lee, Y. Lim, E.A. Lee, H.J. Hwang, J.-W. Moon, J. Power Sources 157 (2006) 848–854.
[23] M.J. Jørgensen, S. Primdahl, C. Bagger, M. Mogensen, Solid State Ionics 139 (2001) 1–11.
[24] X. Xu, Z. Jiang, X. Fan, C. Xia, Solid State Ionics 177 (2006) 2113–2117.